processes

MDPI

*Article*

# The Application of Hydroxyapatite NPs for Adsorption Antibiotic from Aqueous Solutions: Kinetic, Thermodynamic, and Isotherm Studies

**Huda S. Alhasan [1], Suhad A. Yasin [2,*], Nadiyah Alahmadi [3] and Ahmad Khalaf Alkhawaldeh [4]**

[1] Environmental Research and Studies Center, University of Babylon, Hilla 51002, Iraq
[2] Department of Chemistry, College of Science, University of Duhok, Duhok 42001, Iraq
[3] Department of Chemistry, College of Science, University of Jeddah, Jeddah 21959, Saudi Arabia
[4] Department of Allied Medical Sciences, Faculty of Zarqa College, Balqa Applied University, Salt 19110, Jordan
* Correspondence: suhad.yasin@uod.ac

**Abstract:** Antibiotic pollution has become a serious concern due to the extensive use of antibiotics, their resistance to removal, and their detrimental effects on aquatic habitats and humans. Hence, developing an efficient antibiotic removal process for aqueous solutions has become vital. Amoxicillin (Amox) is one of the antibiotics that has been efficiently removed from an aqueous solution using hydroxyapatite nanoparticles (HAP NPs). The current study synthesizes and utilizes hydroxyapatite nanoparticles as a cost-effective adsorbent. Adsorbent dose, pH solution, initial Amox concentration, equilibrium time, and temperature are among the factors that have an evident impact on Amox antibiotic adsorption. The (200) mg dose, pH (5), temperature (25) °C, and time (120) min are shown to be the best-optimized values. The nonlinear Langmuir's isotherm and pseudo-second-order kinetic models with equilibrium capacities of 4.01 mg/g are highly compatible with the experimental adsorption data. The experimental parameters of the thermodynamic analysis show that the Amox antibiotic adsorption onto HAP NPs powder is spontaneous and exothermic.

**Keywords:** adsorption; amoxicillin; hydroxyapatite NPS; kinetic and thermodynamic studies



**Citation:** Alhasan, H.S.; Yasin, S.A.; Alahmadi, N.; Alkhawaldeh, A.K. The Application of Hydroxyapatite NPs for Adsorption Antibiotic from Aqueous Solutions: Kinetic, Thermodynamic, and Isotherm Studies. *Processes* **2023**, *11*, 749. https://doi.org/10.3390/pr11030749

Academic Editors: Elsayed Gamal Zaki and Shymaa Mohamed Elsaeed

Received: 26 January 2023
Revised: 21 February 2023
Accepted: 25 February 2023
Published: 2 March 2023



## 1. Introduction

Antibiotics are one of the few medications that primarily target bacteria, including infections, yet they cause little harm to human tissues and cells [1]. Antibiotics can be classified based on their mechanisms of action or chemical structures. In human and veterinary medicine, more than 250 antibiotic entities have been approved [2]. These antibiotics have been used as potent medications for treating and preventing infections and infection-related illnesses in animals and humans for decades [3]. Antibiotics are rapidly expanding worldwide, attracting increasingly significant attention [4]. The antibiotic residue in the environment is of particular concern because prolonged low-level exposure can result in antibiotic-resistant genes (ARGs) [5]. The extensive use of antibiotics in the past and present has led to substantial residues being transported into terrestrial and aquatic habitats either indirectly or directly [6]. Antibiotic residues from humans and animals have been discovered in various matrices [7–9]. Antibiotics have different half-lives in the environment; a few are exceptionally long, resulting in rising levels of environmental contamination [10]. Many investigations reveal that antibiotic exposure (µg/L-mg/L) has significantly affected the aquatic growth, survival, and body weight of different species [11–13]. Typically, they are released into natural water bodies via pharmaceutical manufacturing effluents and sewage treatment plant effluents [14]. Due to their classification as recalcitrant bio-accumulative compounds, pharmaceutical chemicals, notably antibiotics, are identified as emerging environmental pollutants [15,16]. Antibiotics are hazardous and poisonous [17]. Amoxicillin (Amox) is one of the semisynthetic, broad-spectrum antibiotics routinely

used to treat common human infections. It is a beta-lactam antibiotic with a molecular weight of 365.4 g/mol and a molecular formula of $C_{16}H_{19}N_3O_5S$ [18]. Its antibacterial activity is connected with the beta-lactam ring system in its structure. Blocking connections between the linear peptidoglycan chains hinders bacterial cell wall synthesis [19]. The researchers in Greece investigated the impacts of $TiO_2$/UV-A on Amox and concluded that the applied technique was acceptable [20]. The photocatalytic ozonation was used to conduct rapid mineralization and detoxification of diclofenac and Amox. Such methods were applied in the treatment of urban wastewater [21]. Modern oxidation approaches convert antibiotic molecules into simple complexes or fully mineralize them. However, they are prohibitively costly and too complicated to be sustainably applied to eliminate chemicals such as antibiotics on an industrial scale [22]. Physicochemical technologies have emerged as a viable option for treating organic pollutants [23]. Adsorption, dissimilar to biologically based processes, is easy-to-design, highly efficient, simple to operate, relatively inexpensive, and unaffected by possible toxicity [24]. However, around 30 antibiotics have only been documented utilizing adsorption techniques to extract organic pollutants from contaminated streams onto adsorbent surfaces [25,26].

Nevertheless, this method's most widely used adsorbents are activated carbons (GACs), which are expensive in terms of industry costs. Therefore, there has been a growing interest in identifying easy-to-use alternative adsorbents. Nanoparticles (NPs) are efficient antimicrobials and may be employed as photocatalysts, adsorbents, and membrane materials [27–30].

Chemical and physical processes are used for designing and manufacturing nanostructures [31,32]. Recently, green NP synthesis has risen as an environmentally acceptable and cost-effective alternative to chemical and physical approaches [33].

Nanoparticles have been utilized in the removal of amoxicillin. Pham et al. reported the synthesis and characterization of core–Shell ZnO@$SiO_2$ adsorbent for amoxicillin removal [34]. Machado et al. applied iron nanoparticles to the degradation of amoxicillin [35]. Gaim and his co-workers have invested in the photocatalytic degradation of amoxicillin with Mn-doped $Cu_2O$ nanoparticles [36]. Hydroxyapatite (HAP) [$Ca_{10}$ $(PO_4)_6$ $(OH)_2$] was widely used as an adsorbent in several applications due to its eco-friendliness, biocompatibility, low solubility in water, high adsorption efficiency for heavy metals, good stability within the oxidized and reduced processes, and wide surface area [37–39]. Hydroxyapatite NPs have been applied to remove water pollutants such as organic dyes and antibiotics [40,41]. Moreover, hydroxyapatite has been reported in the literature as a nanocarrier in drug delivery [42,43]. Amoxicillin was loaded onto hydroxyapatite [43,44].

This study aims to investigate the functional activity of HAP NPs, synthesized from eggshells, i.e., biowaste (food waste), in removing Amox from aqueous solutions, taking advantage of the excellent properties of hydroxyapatite nanoparticles, their biocompatibility, and their ability to adsorb many chemicals. The thermodynamics, kinetics, and isotherm parameters are evaluated. In addition, the impact of the experimental conditions, such as pH, contact time, temperature, initial concentrations upon Amox adsorption, and the removal efficiency of Amox utilizing HAP NPs, is investigated.

## 2. Experimental

### *2.1. Materials and Reagents*

In the present study, all solvents and chemical materials have unpurified analytical reagent grades. An amount of 200 µg/mL of amoxicillin trihydrate stock solution (Figure 1) was prepared in deionized water (DI) (Aldrich Chemical Co. Ltd., Milwaukee, WI, USA). Additional diluted standard (10–60 µg/mL) solutions were prepared by diluting the stock solution with deionized water and kept in the refrigerator for a month or less before being used to avoid decomposition. The pH of the final solution was adjusted for all experiments using (0.1 mol/L) of HCl and NaOH.

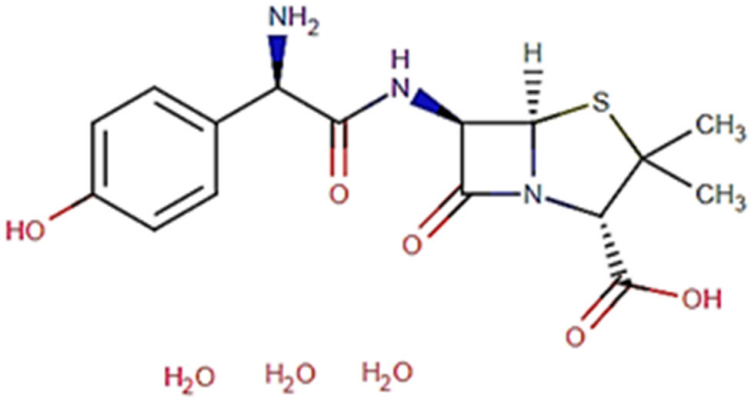


**Figure 1.** Structure of amoxicillin trihydrate.

### 2.2. Apparatus

A Hanna pH meter (301 models) was used to adjust the solutions and measure the pH. A Perkin-Elmer UV–vis (190 nm–1100 nm) spectrophotometer (model Lambda 25, USA) with a 10 mm (path width) quartz cell was employed to record all of the spectrophotometric readings. The ADP 110 L, a digitally sensitive balance with three decimal numbers, was also utilized. All solutions were prepared using deionized water from the Milli-Q Plus system (Millipore, Bedford, MA, USA).

### 2.3. Preparations of HAP-NPs

Calcined eggshells as a calcium basis and (97%) phosphoric acid as a phosphate source were used in the preparation of HAP NPS. Eggshell wastes were collected and then purified using deionized water (DI). The eggshells were dried for 24 h in an oven at 100 °C to eliminate odors and other contaminants, then milled and sieved in a 350 µm sieve. The eggshells were calcined in a furnace at 900 °C for (3) hours at a (10 °C/min) heating rate. In this operation, calcium carbonate ($CaCO_3$) was converted into calcium oxide (CaO) [45]. Subsequently, a 0.3 M suspension solution was prepared by mixing CaO with DI. The resultant solution was used in a wet chemical precipitation reaction by adding $H_3PO_4$ dropwise to the suspension solution. This process involved adjusting the pH to 10 using an $NH_4OH$ solution.

The reaction was mixed for (6 h) at (120 °C) to obtain a homogeneous solution. Then, the suspension was filtered before being washed with DI and dried at 100 °C for 24 h. The outcome was calcined for 2 h at 900 °C. The synthesized powder was grounded and sieved through a mesh size of (0.350 mm) to save homogeneous particles [46,47].

### 2.4. Characterization Techniques

X-Ray Diffraction (XRD) and Transmission Electron Microscopy (TEM) were used to characterize the prepared HAP NPs studied in our previous work [40]. The crystal phase was determined using a Siemens D-5000 XRD equipped with Cu-Kα (λ = 0.154 nm). The shape and size of the HAP were measured using a TEM (JEM 20 Japan) at 200 kV.

### 2.5. Batch Adsorption Experiments

An aqueous solution (25 mL) containing Amox (30 mg/L) in pH = 5 was used to balance the precise weight (0.2 ± 0.01 g) solid phase of the HAP-NPs. A mechanical shaker was utilized to shake the sample solutions for 120 min. The residue concentration of amoxicillin in the solution was measured using a (UV–Vis) spectrophotometer at (227 ± 2 nm) [48]. The separation efficiency percentage (*%E*) and the quantity of Amox adsorbed ($q_t$) per unit mass of HAP solid-phase were calculated using Equations (1) and (2), respectively.

$$\% E = \frac{C_o - C_t}{Co} \times 100 \quad (1)$$

$$q_t = \frac{(C_o - C_t)\ V}{m} \quad (2)$$

$C_o$ represents the initial concentration of Amox, and $C_t$ represents the remaining Amox concentration in the solution after shaking.

## 3. Results and Discussion

### *3.1. Characterizations of HAP NPs*

X-Ray Diffraction (XRD) and Transmission electron microscopy (TEM) were used to characterize the prepared HAP NPs studied. All the results were analyzed in our previous work [43].

### *3.2. Retention of Amox from Aqueous Solutions on HAP*

The solution's pH is one of the essential parameters for studying the adsorption of heavy metal ions and pollutants. After shaking for 120 min at room temperature, the adsorption profile of aqueous solutions that contain Amox at various pH levels via the HAP solid phase was investigated. The quantity of Amox in the aqueous phase after equilibrium was measured using photometry [48]. The adsorption percentage %E of Amox onto HAP increases significantly with the rise in the solution pH up to 5 and then decreases with an increase in the pH, as shown in the representative data (Figure 2). The mechanism of amoxicillin absorption by hydroxyapatite can be explained by several physical processes, such as ion exchange. An exchange may occur between the hydroxyapatite and the protonated functional groups of amoxicillin, such as carboxylate, amine, and hydroxyphenyl. Since amoxicillin has a positive charge at low pH, the adsorption of amoxicillin on hydroxyapatite increases when the pH of the solution increases from 2 to 6, due to the amoxicillin charge shifting to neutral molecules. On the contrary, the absorption of amoxicillin decreases when the pH increases from 7 to 10 as a result of changing the amoxicillin charge to negative [49,50]. Subsequently, pH = 5 is chosen as the best-optimized pH value for the current research work.

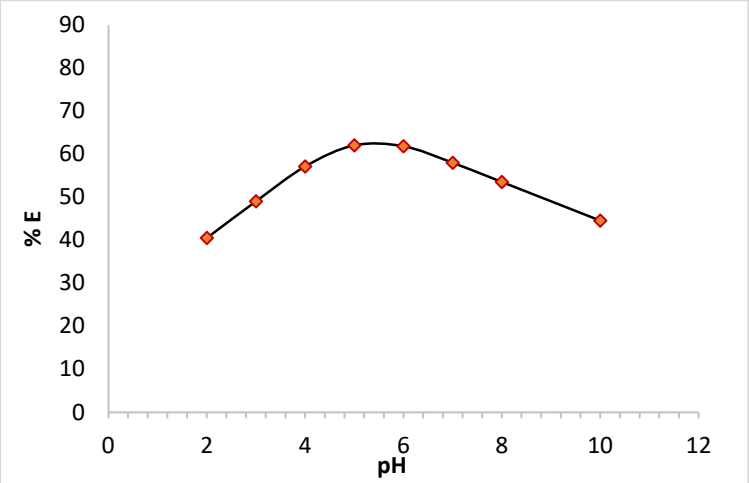


**Figure 2.** Effects of pH solution on Amox adsorption percentage from the aqueous solutions using (0.2 ± 0.01 g) HAP and shaking for 120 min at 25 ± 0.1 °C.

At the 30 mg/L concentration, the impact of the solid-phase HAP mass on the ratio of Amox adsorbed from the solution has been investigated (Figure 3). The figure shows that the HAP proportion eliminated from the aqueous solution ranges from 22.5% to 93.5% when the HAP dose rises from 50 mg to 600 mg. The high amount of solid phase increases the availability of more active sites for adsorption, resulting in a rise in the percentage. In this study, 200 mg of HAP, equivalent to 63.3%, were used to observe the influence of other parameters on adsorption.

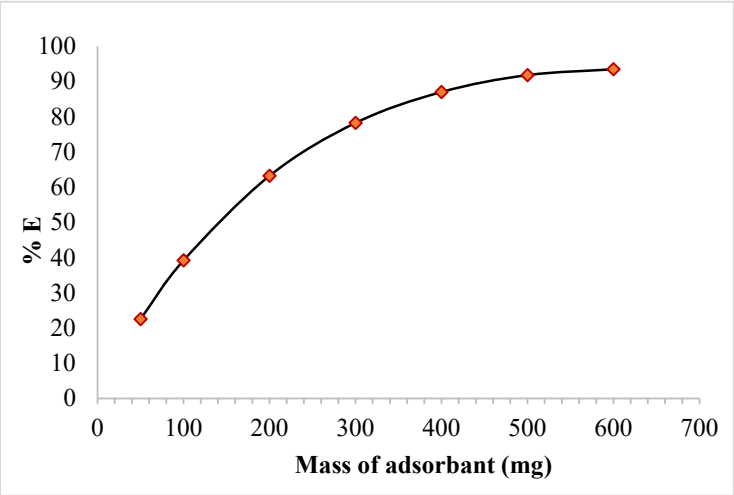


**Figure 3.** Effects of pH solution on Amox adsorption percentage from the aqueous solutions on (0.2 ± 0.01 g) HAP with shaking time 120 min at 25 ± 0.1 °C.

The contact time between an adsorbent and its adsorbate represents one of the critical factors in the adsorption ability to remove pollutant substances. The impact of contact time upon Amox elimination via HAP has been examined, and the results are presented in Figure 4. The steepness of the graph depicts how the increasing contact time results in an increasing process of adsorption. This impact is most noticeable within the first 75 min, when most Amox is physically absorbed (dotted parallel lines). Within 120 min, the proportion of Amox elimination reaches equilibrium. This suggests that Amox adsorption on HAP progresses in two phases, the first of which is the fastest and includes the Amox transfer from the aqueous phase to the external surface of the HAP. The diffusion of Amox between the HAP bundles under the chemical interaction gradient is the second stage, which takes a longer time, thereby representing chemical absorption or adsorption (solid, parallel lines).


The temperature profile at a constant contact time duration is also studied in terms of solution temperature impact on adsorption capability at different optimized temperature values (K) (288, 298, 308, and 323). It is found that the rise in the solution temperature from 288 to 323 K results in a considerable reduction in the Amox adsorption percentage extracted by the HAP (Figure 5). These findings show that the instant adsorption is exothermic and has a negative Gibbs free energy value, thereby showing the spontaneity of the overall adsorption process.

The retention profile of Amox from aqueous solutions with a pH of 5 is examined over a broad range of equilibrium values (10 mg/L–60 mg/L). In (Figure 6), %E of Amox species adsorbed onto HAP is shown against the corresponding concentration in the aqueous solution. More dilute aqueous solutions produce the most favorable %E of Amox adsorption onto HAP sorbent. With the rising Amox concentrations, the %E values decline, and the HAP membranes become increasingly saturated with the retained Amox species.

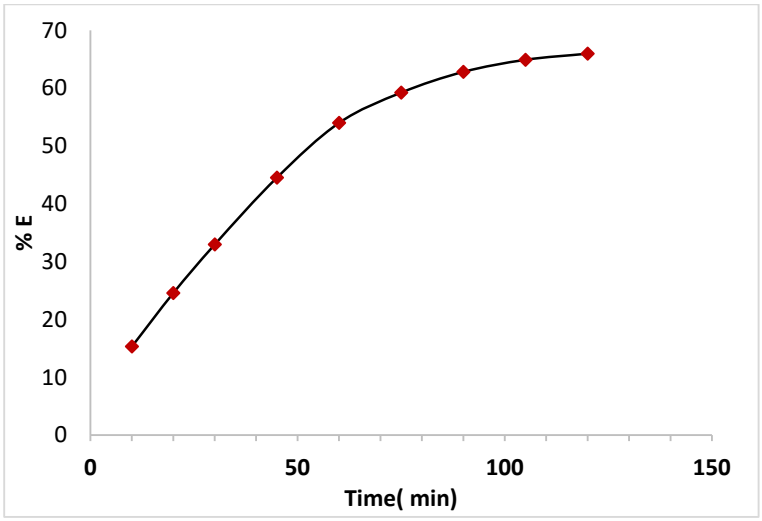


**Figure 4.** Effects of shaking time upon adsorption percentage of Amox (30 mg/L) from aqueous solutions onto (0.2 ± 0.01 g) HAP at 25 °C and pH 5.

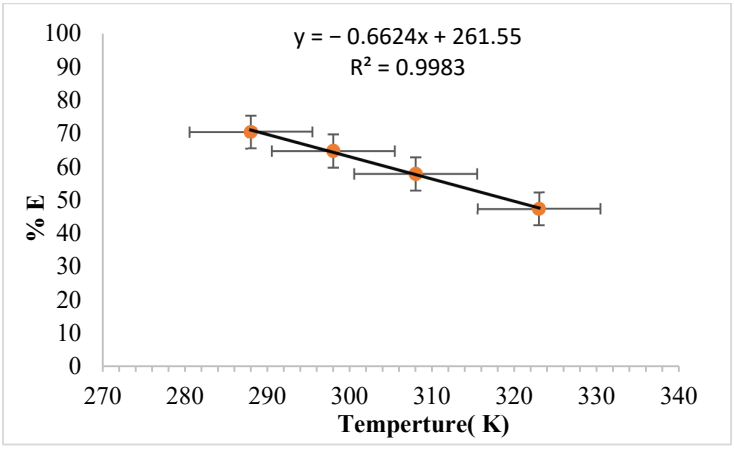


**Figure 5.** Effects of temperature on the percentage of Amox removal from solutions onto (0.2 ± 0.01 g) HAP at 288, 298, 308, and 323 K; pH 5; shaking time 120 min.

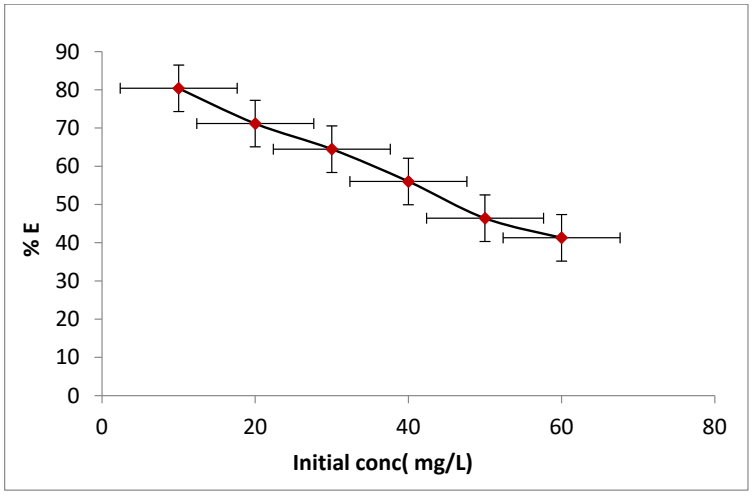


**Figure 6.** Effects on initial concentration upon removal Amox percentage from aqueous solutions onto (0.2 ± 0.01 g) HAP at 25 °C; pH 5; shaking time 120 min.

### *3.3. Kinetic of Amox Adsorption on HAP solid Phase*

The adsorption kinetics of pollutants such as those of the Amox species from aqueous solutions through the solid sorbent are essential. It delivers important insights into the reaction pathways and net adsorption. The retention of Amox species adsorption on the solid-phase HAP depends on intra-particle and film diffusion. The more rapid one controls the overall transport rate [51]. Based on the effect of shaking time, the study conclusions have been supported by calculating the ($t^{1/2}$) half-life time of the Amox adsorption from solutions onto HAP of solid sorbent. The ($t^{1/2}$) values are estimated based on log $C/C_o$ plots vs. the time of Amox adsorption onto HAP. The ($t^{1/2}$) value is 1.60 ± 0.04 min and agrees with the ($t^{1/2}$) values reported previously [52,53]. This is why the kinetics of Amox species adsorption onto HAP adsorbent depend on the film and intra-particle diffusion, where a more rapid one can control the overall transport rate. The Amox species sorbed onto the HAP sorbent, which was subjected to investigation using the Weber–Morris model [54]:

$$q_t = R_d(t)^{1/2} \quad (3)$$

$R_d$ and $q_t$ represent the intra-particle transport rate constant and sorbed Amox concentration at the time, respectively. The $q_t$ against the time plot has been depicted (Figure 7). The $R_d$ values calculated from distinct Weber–Morris plot slopes (Figure 7) equal 0.27 with ($R^2$ = 0.986) as a correlation coefficient.

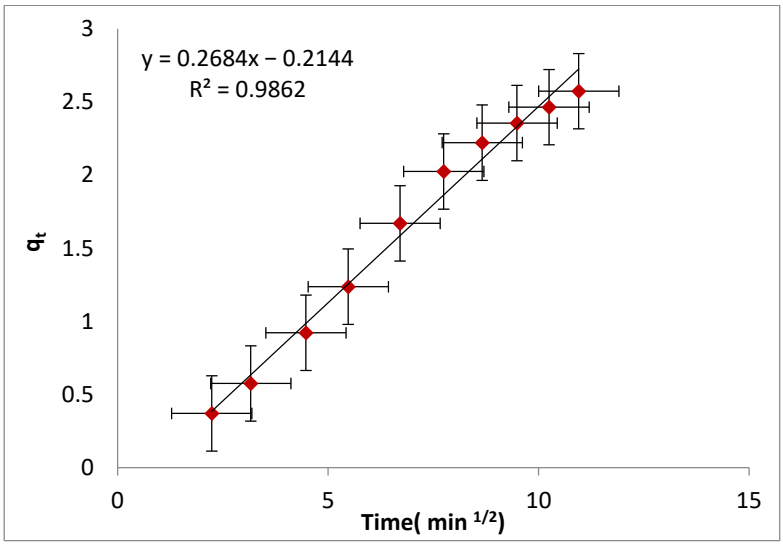


**Figure 7.** Weber–Morris plot of adsorbed Amox from the aqueous solutions onto the HAP vs. the value of the square root of the time.

The kinetic model of a fractional power function modified from Freundlich's equation can be represented by the following relation [55]:

$$ln\ q_t = ln\ a + b\ ln\ t \quad (4)$$

$q_t$ refers to the amount of the Amox species adsorbed per HAP unit mass (mg/g) at a time ($t$), and ($a$ and $b$) represent coefficients with $b < 1$. The experimental data from the adsorption process apply to the fractional power equation (Figure 8).

The values of (a and b) are displayed in Table 1, and the data are consistent with the coefficient of correlation ($R^2$) value of 0.988.

The data also indicate that the kinetic model does not apply to the description of Amox adsorption by HAP.

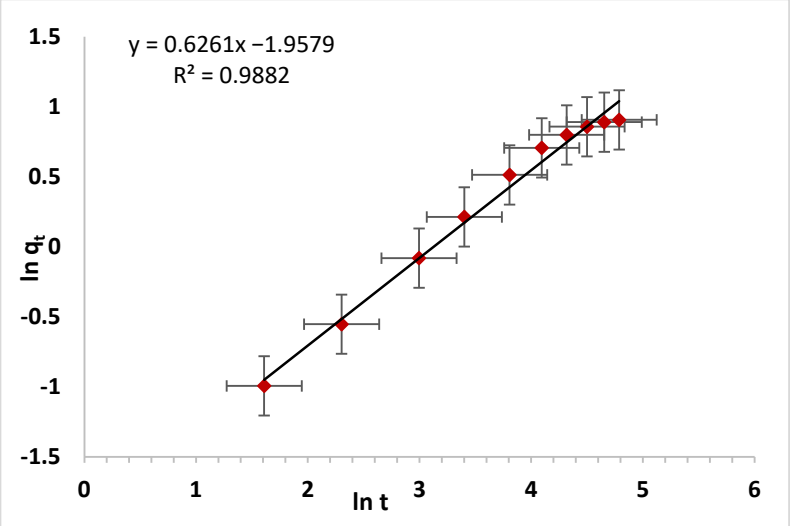


**Figure 8.** Fractional power model plots of Amox from the aqueous solutions onto the HAP.

Adsorption rates in liquid-phase systems are described by the common Lagergren equation. The variation of the adsorption of Amox species from an aqueous medium onto the solid phase of HAP is subjected to Lagergren's equation [56]:

$$log\ (q_e - q_t) = log\ q_e - k_{lager}t/2.303 \quad (5)$$

The adsorption of Amox per sorbent unit mass is represented by ($q_e$). For the retention process, ($K_{Lager}$) represents a general rate constant of the first order, and (t) denotes time. The log ($q_e - q_t$) vs. time plot (Figure 9) is linear, and ($K_{Lager}$) and the calculated ($q_e$) values are (0.039 $min^{-1}$) and (3.49 mg/g), respectively, with the correlation coefficient ($R^2$ = 0.973). The resulting data do not agree with the first-order adsorption kinetics of Amox onto (HAP) as a solid sorbent [57].

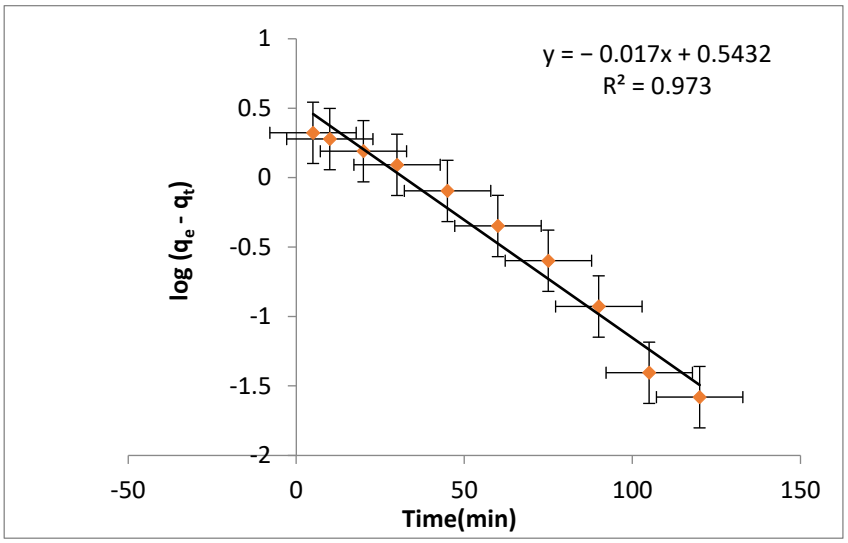


**Figure 9.** Lagergren model of Amox uptake onto HAP vs. time.

A pseudo-second-order equation is utilized, as well as a particular kinetics model [53], supported on the assumption that:

(a) The amount of adsorbate in the solution remains constant over time;
(b) In an equilibrium state, the amount of adsorbate adsorbed determines the whole number of binding sites.

A linearized pseudo-second-order rate form is represented in the below equation:

$$\frac{t}{qt} = \frac{1}{h} + \left(\frac{1}{qe}\right)t \quad (6)$$

($h = k_2 q_e^2$ relates to the rate of initial adsorption, and ($qe$ and $qt$) denote the adsorbed quantities per unit mass at any time (t). In these conditions, ($t/qt$) vs. (t) plots are linear (Figure 10). The ($k_2$) is a second-order rate constant, and the equilibrium capacity ($q_e$) for the Amox species is computed from the intercept and slope. They are equal to ($3.9 \times 10^{-3}$ g) (mg. min)$^{-1}$ and (4.01 mg/g), with a notable degree of correlation ($R^2 = 0.996$). The data show that all of the experimental data fit well with the excellent agreement values and the pseudo-second-order rate constants, $k_2$, which typically depend on the experimental conditions.

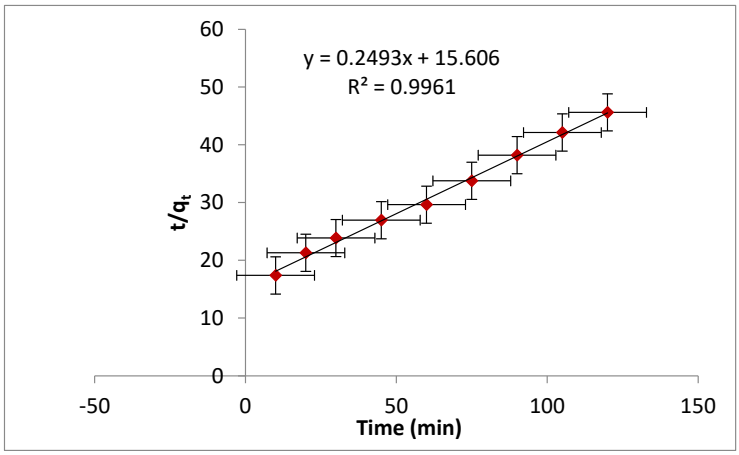


**Figure 10.** Pseudo-second order of Amox uptake onto HAP vs. time.

The rate equation is formulated based on the capacity of adsorption that is typically described by the Elovich model [58]. The latter is mainly applicable for the chemisorption kinetics and valid for systems with heterogeneous adsorbing surfaces. The below equation represents the model:

$$qt = \beta\, ln\, (\alpha\beta) + \beta\, ln\, t \quad (7)$$

The α (g·mg$^{-1}$ min$^{-1}$) and β (mg·g$^{-1}$ min$^{-1}$) stand for the initial adsorption rate and the desorption coefficient, respectively. The ($q_t$) versus (lnt) plot is linear (Figure 11). The figure shows that the parameters of the Elovich equation α and β calculated from intercepts and slopes for Amox are (0.20 g·mg$^{-1}$ min$^{-1}$) and (0.84 mg·g$^{-1}$ min$^{-1}$), respectively, with ($R^2 = 0.983$).

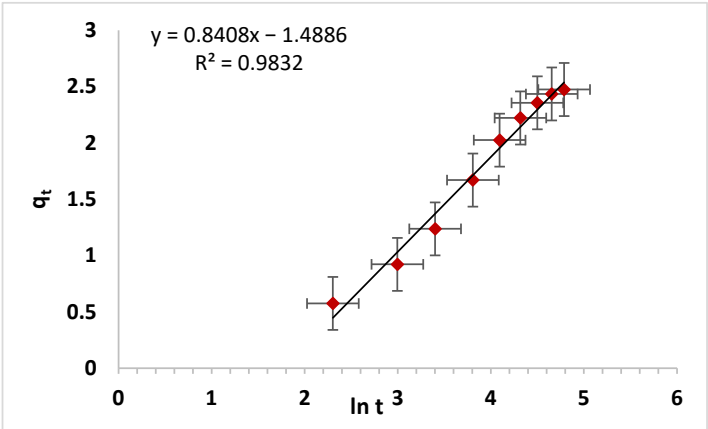


**Figure 11.** Elovich model plot for Amox uptake onto HAP vs. time.

Based on kinetic data, it was determined that the pseudo-second-order kinetic model is the most fitting for explaining the adsorption of Amox by HAP from the solution, which has been shown in Table 1.

**Table 1.** The parameters of various kinetic models for Amox adsorption on HAP at 298 K.

| | | | | |
|---|---|---|---|---|
| | Weber–Morris model | | | |
| | $R_d$ | | | $R^2$ |
| Amox | 0.27 | | | 0.986 |
| | Fractional power function kinetic models | | | |
| | A | B | ab | $R^2$ |
| Amox | 0.141 | 0.626 | 0.088 | 0.988 |
| | The pseudo-first-order kinetic (lagregen) model | | | |
| | $q_{e,\,exp}$ (mg/g) | $q_{e,\,calc}$(mg/g) | $k_1$ | $R^2$ |
| Amox | 2.47 | 3.49 | 0.039 | 0.973 |
| | The pseudo-second-order kinetic models | | | |
| | $q_{e,\,exp}$ (mg/g) | $q_{e,\,calc}$(mg/g) | $k_2$ | $R^2$ |
| Amox | 2.47 | 4.01 | $3.9 \times 10^{-3}$ | 0.996 |
| | Elovich kinetic model | | | |
| | α, (g/mg min) | β, (mg/g min) | | $R^2$ |
| Amox | 0.2 | 0.84 | | 0.983 |

### *3.4. Adsorption Isotherms*

The models of adsorption isotherms are applied to describe the Amox interaction mechanism on the surface of the adsorbent. The equilibrium studies are valuable for calculating the highest HAP adsorption capacity towards Amox and determining the extensive surface features of the tested sorbent. A critical investigation is carried out to study the profiles of the retention over a range of concentrations (10 mg/L–60 mg/L) from Amox solutions on the used sorbent at optimum conditions.

The plot of the Amox amount adsorbed onto HAP vs. the Amox concentration values in solution is depicted in (Figure 12). At moderate concentrations of the analyte, the amount of Amox retained on the HAP linearly varies with the amount of Amox that remains in the solution. A ($3.10 \pm 0.05$ mg $g^{-1}$) adsorption capacity of Amox onto HAP is achieved.

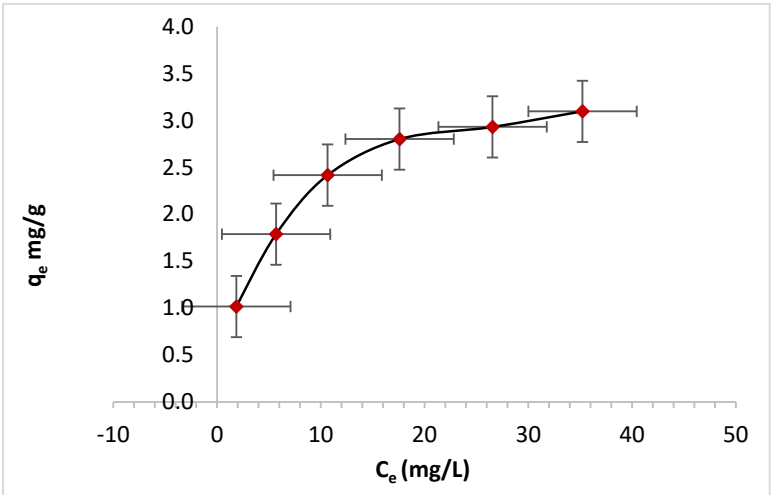


**Figure 12.** A plot of Amox retained ($q_e$) onto HAP (mg/g) vs. equilibrium concentration ($C_e$); at $25 \pm 1$ °C.

The adsorption of Amox onto the sorbent (HAP) is subjected to the model of Langmuir isotherm represented in the linear form below [58]:

$$\frac{C_e}{C_{ads}} = \frac{1}{Qb} + \frac{C_e}{Q} \quad (8)$$

*Ce* refers to the concentration (mg/L) of Amox in the analysis solution, and $C_{ads}$ represents the Amox amount that has been retained on HAP (per unit mass). The Q and b constants represent Langmuir's parameters related to the solute's maximum adsorption capacity per unit of adsorbent. These parameters are needed for surface monolayer coverage. The equilibrium constant is related to the binding energy of the solute's adsorption. The $C_e/C_{ads}$ against $C_e$ plot over the entire Amox concentration range onto HAP is linear ($R^2$ = 0.998). The linearity indicates that the Amox adsorption onto the HAP follows the Langmuir model (Figure 13). Q and B values calculated from the linear plot slope and intercept are equal: (3.92 ± 0.03 mmol/g) and (0.11 ± 0.01 L/mol), respectively.

The behavior of the Amox retention from the solution on the deployed types of the sorbent is subjected to the Freundlich model, which can be represented by the linear form below [59]:

$$log\ q_e = log\ A + \frac{1}{n}\ log\ C_e \quad (9)$$

($A$) and ($1/n$) represent the Freundlich parameters related to the highest solute adsorption capacity (mg/g), $q_e$ denotes the retained Amox onto the HAP concentration (mg/g) at equilibrium, and $C_e$ represents the Amox concentration in the solution (mg/L) (Figure 14). The parameters ($A$ and $1/n$) of Freundlich are estimated based on the slope, and the intercept is equal to (0.47) and (0.63) ($R^2$ = 0.964). The data show that there is unfavorable adsorption of Amox by HAP and that the model used is undoubtedly improper to fit well with the data.

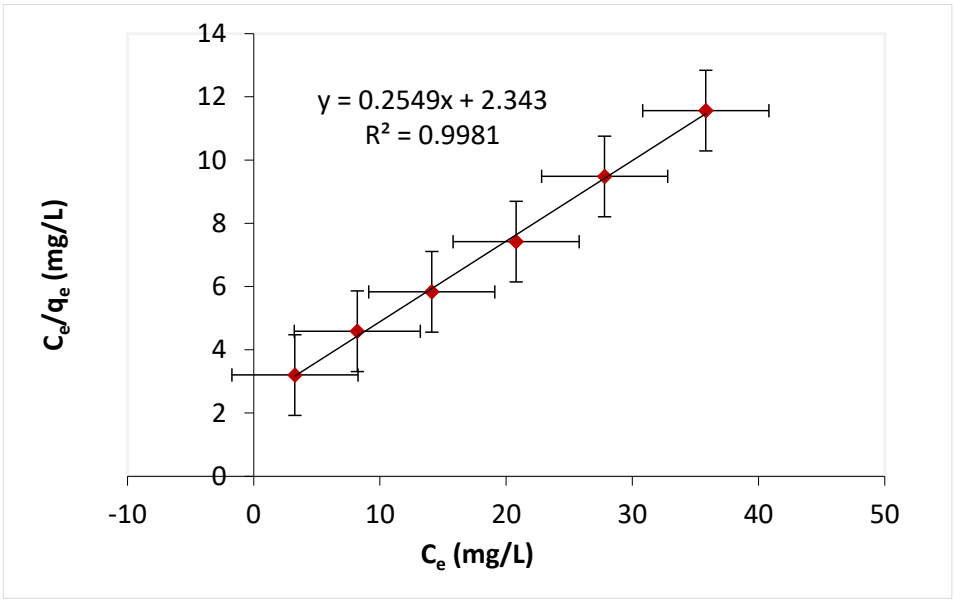


**Figure 13.** Langmuir's adsorption isotherms of the Amox aqueous solutions onto HAP at 25 ± 1 °C.

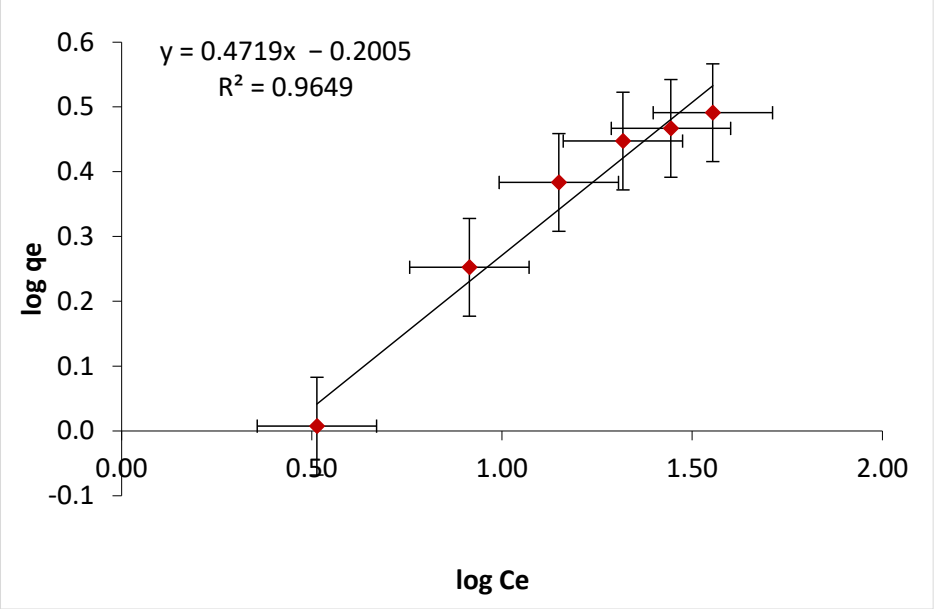


**Figure 14.** log $q_e$ vs. log $C_e$ plot of Amox retention on HAP at 25 ± 1 °C (Freundlich isotherms).

*3.5. Thermo-Dynamic Features of Amox Retention on HAP*

The Amox adsorption onto the HAP solid phase is essential. It has been researched over many different temperatures (288–323 K) to determine the Amox retention on the HAP. The thermo-dynamic parameters (ΔS, ΔH, and ΔG) are assessed using equations (10, 11 and 12) [60]:

$$ln\ K_c = \frac{-\Delta H}{RT} + \frac{\Delta S}{R} \quad (10)$$

$$\Delta G = \Delta H - T\Delta S \quad (11)$$

$$\Delta G = -RT\ ln\ K_c \quad (12)$$

$\Delta H$, $\Delta S$, and $\Delta\ G$ are the enthalpy, entropy, and Gibbs free energy variations. $T$ denotes the degree of temperature (Kelvin), R represents a value of the gas constant (approximately 8.314 $J{\cdot}K^{-1}$ $mol^{-1}$), and ($K_C$) stands for the equilibrium constant. The ($K_C$) values for the Amox adsorption from the solution at equilibrium onto solid sorbent are calculated according to the equation below:

$$k_c = \frac{Ca}{Ce} \quad (13)$$

($C_e$) is the Amox concentration at equilibrium in solution (mg $L^{-1}$), and ($C_a$) is the amount of Amox adsorbed on the adsorbate per liter at equilibrium (mg $L^{-1}$). The ln $K_C$ versus (1000/T) plot is linear over a range of temperature degrees (288–323 K) (Figure 15). The equilibrium constant decreases with an increase in temperature. This direct, proportional increase reveals that the Amox retention process on utilized sorbent materials is exothermic. The ΔH, Δ S, and ΔG numerical values for the release of Amox calculated from the slope and intercept of the (ln $K_C$) versus (1000/T) linear plot are (−21.53 ± 0.1 kJ/mol), (−67.51 ± 0.2 J $mol^{-1}$ $K^{-1}$), and (−1.42 ± 0.08 kJ $mol^{-1}$) at 298 K temperature (Figure 15). The negative ΔH value has revealed the exothermic nature of the uptake process. The negative value of ΔS proves that the step of the re-orientation is entropy, and it is regulated at the state of the activation, indicating non-electrostatic bonding of the adsorbent phase and solid phase. However, the negative value of ΔG at 298 K for the formed solid phase indicates the spontaneous nature of the adsorption of Amox onto HAP. Table 2 shows the comparison of adsorption conditions with those of other adsorbents reported in the literature.

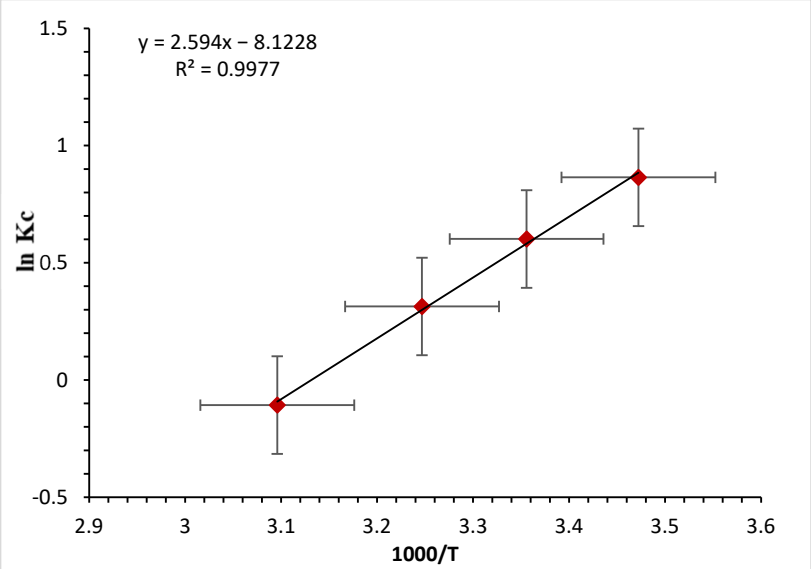


**Figure 15.** ln $K_C$ of Amox adsorption plot from an aqueous medium onto HAP vs. 1000/T.

## 4. Conclusions

The present research indicates that the HAP nanoparticle is an appropriate adsorbent for eliminating the Amox antibiotic from the aqueous solution. The HAP adsorbent's performance is highly influenced by many parameters, such as contact time, Amox temperature, the concentration of adsorbate, adsorbent dosage, and initial pH. The Langmuir isotherm fits the equilibrium data on the adsorption of Amox compared with the Freundlich model, which indicates monolayer adsorption with a maximal capacity of 4.01 mg/g of HAP at 25 °C and a pH of 5. The Amox adsorption onto HAP is well-fitted to the pseudo-second-order kinetic model. The results of the thermo-dynamic study indicate the physisorption process. The estimated thermo-dynamic parameters have shown that the adsorption process is spontaneous and exothermic. Overall, the current study's findings propose that the HAP nanoparticles can be used as effective and ecologically acceptable adsorbents for removing the Amox antibiotic from aqueous solutions.

**Table 2.** Comparison of adsorption conditions with other adsorbents reported in the literature.

| | Adsorbent | Conditions | Refs. |
|---|---|---|---|
| 1 | $ZnO@SiO_2$ | 10 mg/L Amox, 25 mg/mL of $ZnO@SiO_2$ at pH 8 | [34] |
| 2 | ZnO@CNF nanoadsorbent | 25 mg/L of Amox, 0.09 g of ZnO@CNF at pH7.5 | [61] |
| 3 | $Fe_3O_4$@C nanoparticles | 50 to 300 mg/L of Amox, 1 g/L $Fe_3O_4$@C at pH 5 | [62] |
| 4 | Maltodextrin/reduced graphene/CuO nanocomposite | 30 mg/L of Amox, 0.05 g of nanocomposite at a pH of 7.4 | [63] |
| 5 | Ag NPs | 30 mg/L of Amox, 0.5 of Ag NPs at pH 4 | [64] |
| 6 | $Fe_3O_4$-chitosan/Ag NPs | 20 mg/L of Amox, 0.4 g/L $Fe_3O_4$-chitosan/Ag NPs at pH 4 | [65] |
| 7 | $Fe_3O_4$@AgNPs | 100 and 500 µL of Amox, 10 and 100 mg/L of $Fe_3O_4$@AgNPs at pH 7 | [66] |
| 8 | $MoS_2$ Nanosheets | 45.2 µg/mL of Amox, 1.5 mg/mL of $MoS_2$ Nanosheets at pH 10.2 | [67] |
| 9 | Bismuth oxyiodide-chitosan (BiOI-Ch) bionanocomposite | 80 mg/g of Amox, 1.7 g/L of BiOI-Ch at pH 3 | [68] |
| 10 | Hydroxyapatite HAP | 30 mg/L of Amox, 4.01 mg/g of HAP at pH 5 | This study |

**Author Contributions:** Conceptualization, H.S.A. and S.A.Y.; methodology, H.S.A., S.A.Y. and N.A.; software, S.A.Y.; validation, H.S.A. and S.A.Y.; formal analysis, N.A. and A.K.A.; investigation, H.S.A.; resources, N.A.; data curation, H.S.A. and S.A.Y.; writing—original draft preparation, H.S.A. and A.K.A.; writing—review and editing, H.S.A. and A.K.A.; visualization, H.S.A.; supervision, H.S.A. and S.A.Y.; project administration, H.S.A., S.A.Y. and N.A. All authors have read and agreed to the published version of the manuscript.

**Funding:** This research received no external funding And The APC was funded by the authors themselves.

**Institutional Review Board Statement:** Not applicable.

**Informed Consent Statement:** Not applicable.

**Data Availability Statement:** Not applicable.

**Acknowledgments:** The authors thank the UoD PEER laboratory for supporting this work at the University of Duhok.

**Conflicts of Interest:** The authors declare that there are no competing financial interest.

## References

1. Boddu, R.S.; Perumal, O. Microbial nitroreductases: A versatile tool for Biomedical and Environmental Applications. *Biotechnol. Appl. Biochem.* **2021**, *68*, 1518–1530. [CrossRef] [PubMed]
2. Palmer, N.; Maasch, J.R.; Torres, M.D.; de la Fuente-Nunez, C. Molecular dynamics for Antimicrobial Peptide Discovery. *Infect. Immun.* **2021**, *89*, e00703-20. [CrossRef] [PubMed]
3. Fatahi-Bafghi, M. Antibiotic resistance genes in the actinobacteria phylum. *Eur. J. Clin. Microbiol. Infect. Dis.* **2019**, *38*, 1599–1624. [CrossRef] [PubMed]
4. Zhang, F.; Lin, L.; Xie, J. A mini-review of chemical and biological properties of polysaccharides from Momordica Charantia. *Int. J. Biol. Macromol.* **2016**, *92*, 246–253. [CrossRef]
5. Zainab, S.M.; Junaid, M.; Xu, N.; Malik, R.N. Antibiotics and antibiotic resistant genes (args) global review on dissemination, sources, interactions, environmental and human health risks. *Water Res.* **2020**, *187*, 116455. [CrossRef]
6. Terrado, M.; Sabater, S.; Chaplin-Kramer, B.; Mandle, L.; Ziv, G.; Acuña, V. Model development for the assessment of terrestrial and aquatic habitat quality in conservation planning. *Sci. Total Environ.* **2016**, *540*, 63–70. [CrossRef]
7. Moyo, B.; Gitari, M.; Tavengwa, N.T. Application of sorptive micro-extraction techniques for the pre-concentration of antibiotic drug residues from food samples—A review. *Food Addit. Contam. Part A* **2020**, *37*, 1865–1880. [CrossRef]
8. Ortelli, D.; Spörri, A.S.; Edder, P. Veterinary drug residue in food of animal origin in Switzerland: A health concern? *CHIMIA* **2018**, *72*, 713. [CrossRef]
9. Khataei, M.M.; Epi, S.B.; Lood, R.; Spégel, P.; Yamini, Y.; Turner, C. A review of green solvent extraction techniques and their use in antibiotic residue analysis. *J. Pharm. Biomed. Anal.* **2022**, *209*, 114487. [CrossRef]
10. Tasho, R.P.; Cho, J.Y. Veterinary antibiotics in animal waste, its distribution in soil and uptake by plants: A Review. *Sci. Total Environ.* **2016**, *563–564*, 366–376. [CrossRef]
11. Shin, Y.-J.; Kim, B.; Kim, H.; Kim, K.; Park, K.; Kim, J.; Kim, H.-J.; Kim, P. 1,2,3-benzotriazole adversely affects the early-life stage of Oryzias latipes. *Sci. Total Environ.* **2022**, *815*, 152846. [CrossRef] [PubMed]
12. Martins, N.; Pereira, R.; Abrantes, N.; Pereira, J.; Gonçalves, F.; Marques, C.R. Ecotoxicological effects of ciprofloxacin on freshwater species: Data integration and derivation of toxicity thresholds for risk assessment. *Ecotoxicology* **2012**, *21*, 1167–1176. [CrossRef] [PubMed]
13. Redondo-Hasselerharm, P.E.; Falahudin, D.; Peeters, E.T.; Koelmans, A.A. Microplastic effect thresholds for freshwater benthic macroinvertebrates. *Environ. Sci. Technol.* **2018**, *52*, 2278–2286. [CrossRef] [PubMed]
14. Michael, I.; Rizzo, L.; McArdell, C.S.; Manaia, C.M.; Merlin, C.; Schwartz, T.; Dagot, C.; Fatta-Kassinos, D. Urban wastewater treatment plants as hotspots for the release of antibiotics in the environment: A Review. *Water Res.* **2013**, *47*, 957–995. [CrossRef]
15. Chaturvedi, P.; Shukla, P.; Giri, B.S.; Chowdhary, P.; Chandra, R.; Gupta, P.; Pandey, A. Prevalence and hazardous impact of pharmaceutical and personal care products and antibiotics in environment: A review on emerging contaminants. *Environ. Res.* **2021**, *194*, 110664. [CrossRef]
16. Sungur, Ş. Pharmaceutical and personal care products in the environment: Occurrence and impact on the functioning of the ecosystem. *Emerg. Contam. Environ.* **2022**, 137–157. [CrossRef]
17. Kosutic, K.; Dolar, D.; Asperger, D.; Kunst, B. Removal of antibiotics from a model wastewater by RO/NF membranes. *Sep. Purif. Technol.* **2007**, *53*, 244–249. [CrossRef]
18. Pouretedal, H.R.; Sadegh, N. Effective removal of amoxicillin, cephalexin, tetracycline and penicillin G from aqueous solutions using activated carbon nanoparticles prepared from Vine Wood. *J. Water Process Eng.* **2014**, *1*, 64–73. [CrossRef]
19. Tian, X.; Fei, J.; Pi, Z.; Yang, C.; Luo, D. Synthesis and characterization of amoxicillin nanostructures. *Nanomed. Nanotechnol. Biol. Med.* **2005**, *1*, 323–325. [CrossRef]

20. Dimitrakopoulou, D.; Rethemiotaki, I.; Frontistis, Z.; Xekoukoulotakis, N.P.; Venieri, D.; Mantzavinos, D. Degradation, mineralization and antibiotic inactivation of amoxicillin by UV-A/$TiO_2$ photocatalysis. *J. Environ. Manag.* **2012**, *98*, 168–174. [CrossRef]
21. Moreira, N.F.F.; Orge, C.A.; Ribeiro, A.R.; Faria, J.L.; Nunes, O.C.; Pereira, M.F.; Silva, A.M.T. Fast mineralization and detoxification of amoxicillin and diclofenac by photocatalytic ozonation and application to an urban wastewater. *Water Res.* **2015**, *87*, 87–96. [CrossRef] [PubMed]
22. Mehrjouei, M.; Müller, S.; Möller, D. Energy consumption of three different advanced oxidation methods for water treatment: A cost-effectiveness study. *J. Clean. Prod.* **2014**, *65*, 178–183. [CrossRef]
23. Homem, V.; Santos, L. Degradation and removal methods of antibiotics from aqueous matrices—A Review. *J. Environ. Manag.* **2011**, *92*, 2304–2347. [CrossRef]
24. Zhou, Q.; Li, Z.; Shuang, C.; Li, A.; Zhang, M.; Wang, M. Efficient removal of tetracycline by reusable magnetic microspheres with a high surface area. *Chem. Eng. J.* **2012**, *210*, 350–356. [CrossRef]
25. Han, R.; Ding, D.; Xu, Y.; Zou, W.; Wang, Y.; Li, Y.; Zou, L. Use of rice husk for the adsorption of Congo Red from aqueous solution in Column Mode. *Bioresour. Technol.* **2008**, *99*, 2938–2946. [CrossRef] [PubMed]
26. Ciesielczyk, F.; Bartczak, P.; Klapiszewski, Ł.; Jesionowski, T. Treatment of model and galvanic waste solutions of copper (ii) ions using a lignin/inorganic oxide hybrid as an effective sorbent. *J. Hazard. Mater.* **2017**, *328*, 150–159. [CrossRef]
27. Xu, H.; Zhu, S.; Lu, K.; Jia, H.; Xia, M.; Wang, F. Preparation of hierarchically floral ZIF-8 derived carbon@polyaniline@Ni/Al layered double hydroxides composite with outstanding removal phenomenon for saccharin. *Chem. Eng. J.* **2022**, *450*, 138127. [CrossRef]
28. Bakry, A.M.; Alamier, W.M.; Salama, R.S.; Samy El-Shall, M.; Awad, F.S. Remediation of water containing phosphate using ceria nanoparticles decorated partially reduced graphene oxide (CEO2-PRGO) composite. *Surf. Interfaces* **2022**, *31*, 102006. [CrossRef]
29. Ibrahim, A.A.; Salama, R.S.; El-Hakam, S.A.; Khder, A.S.; Ahmed, A.I. Synthesis of 12-tungestophosphoric acid supported on Zr/MCM-41 composite with excellent heterogeneous catalyst and promising adsorbent of Methylene Blue. *Colloids Surf. A Physicochem. Eng. Asp.* **2021**, *631*, 127753. [CrossRef]
30. Salama, R.S.; El-Hakam, S.A.; Samra, S.E.; El-Dafrawy, S.M.; Ahmed, A.I. Cu-BDC as a Novel and Efficient Catalyst for the Synthesis of 3, 4-Dihydropyrimidin-2 (1H)-ones and Aryl-14H-dibenzo [a, j] Xanthenes under Conventional Heating. *Int. J. Nano Mater. Sci.* **2018**, *7*, 31–42.
31. Fulekar, M.H. Microbial degradation of petrochemical waste-polycyclic aromatic hydrocarbons. *Bioresour. Bioprocess.* **2017**, *4*, 1–16. [CrossRef] [PubMed]
32. Gashtasbi, F.; Yengejeh, R.J.; Babaei, A.A. Photocatalysis assisted by activated-carbon-impregnated magnetite composite for removal of cephalexin from aqueous solution. *Korean J. Chem. Eng.* **2018**, *35*, 1726–1734. [CrossRef]
33. Singh, A.; Gautam, P.K.; Verma, A.; Singh, V.; Shivapriya, P.M.; Shivalkar, S.; Sahoo, A.K.; Samanta, S.K. Green synthesis of metallic nanoparticles as effective alternatives to treat antibiotics resistant bacterial infections: A Review. *Biotechnol. Rep.* **2020**, *25*, e00427. [CrossRef] [PubMed]
34. Pham, T.-D.; Truong, T.-T.-T.; Nguyen, H.-L.; Hoang, L.-B.-L.; Bui, V.-P.; Tran, T.-T.-M.; Dinh, T.-D.; Le, T.-D. Synthesis and characterization of novel core–shell ZnO@$SiO_2$ nanoparticles and application in antibiotic and bacteria removal. *ACS Omega* **2022**, *7*, 42073–42082. [CrossRef]
35. Machado, S.; Pacheco, J.G.; Nouws, H.P.; Albergaria, J.T.; Delerue-Matos, C. Green zero-valent iron nanoparticles for the degradation of amoxicillin. *Int. J. Environ. Sci. Technol.* **2016**, *14*, 1109–1118. [CrossRef]
36. Gaim, Y.T.; Yimanuh, S.M.; Kidanu, Z.G. Enhanced photocatalytic degradation of amoxicillin with MN-doped cu2o under sunlight irradiation. *J. Compos. Sci.* **2022**, *6*, 317. [CrossRef]
37. Sultan, M. Hydroxyapatite/polyurethane composites as promising biomaterials. *Chem. Pap.* **2018**, *72*, 2375–2395. [CrossRef]
38. Ragab, A.; Ahmed, I.; Bader, D. The removal of brilliant green dye from aqueous solution using nano hydroxyapatite/chitosan composite as a Sorbent. *Molecules* **2019**, *24*, 847. [CrossRef]
39. Bee, S.-L.; Hamid, Z.A.A. Hydroxyapatite derived from food industry bio-wastes: Syntheses, properties and its potential multifunctional applications. *Ceram. Int.* **2020**, *46*, 17149–17175. [CrossRef]
40. Alhasan, H.S.; Alahmadi, N.; Yasin, S.A.; Khalaf, M.Y.; Ali, G.A. Low-cost and eco-friendly hydroxyapatite nanoparticles derived from eggshell waste for cephalexin removal. *Separations* **2022**, *9*, 10. [CrossRef]
41. Vinayagam, R.; Pai, S.; Murugesan, G.; Varadavenkatesan, T.; Kaviyarasu, K.; Selvaraj, R. Green synthesized hydroxyapatite nanoadsorbent for the adsorptive removal of AB113 Dye for environmental applications. *Environ. Res.* **2022**, *212*, 113274. [CrossRef] [PubMed]
42. Alotaibi, N.H.; Munir, M.U.; Alruwaili, N.K.; Alharbi, K.S.; Ihsan, A.; Almurshedi, A.S.; Khan, I.U.; Bukhari, S.N.; Rehman, M.; Ahmad, N. Synthesis and characterization of antibiotic–loaded biodegradable citrate functionalized mesoporous hydroxyapatite nanocarriers as an alternative treatment for bone infections. *Pharmaceutics* **2022**, *14*, 975. [CrossRef] [PubMed]
43. Prasanna, A.P.; Venkatasubbu, G.D. Sustained release of amoxicillin from hydroxyapatite nanocomposite for bone infections. *Prog. Biomater.* **2018**, *7*, 289–296. [CrossRef] [PubMed]
44. Zheng, F.; Wang, S.; Wen, S.; Shen, M.; Zhu, M.; Shi, X. Characterization and antibacterial activity of amoxicillin-loaded electrospun nano-hydroxyapatite/poly(lactic-co-glycolic acid) composite nanofibers. *Biomaterials* **2013**, *34*, 1402–1412. [CrossRef] [PubMed]
45. Kamalanathan, P.; Ramesh, S.; Bang, L.T.; Niakan, A.; Tan, C.Y.; Purbolaksono, J.; Chandran, H.; Teng, W.D. Synthesis and sintering of hydroxyapatite derived from eggshells as a calcium precursor. *Ceram. Int.* **2014**, *40*, 16349–16359. [CrossRef]

46. Chaudhuri, B.; Mondal, B.; Modak, D.K.; Pramanik, K.; Chaudhuri, B.K. Preparation and characterization of nanocrystalline hydroxyapatite from egg shell and $K_2HPO_4$ Solution. *Mater. Lett.* **2013**, *97*, 148–150. [CrossRef]
47. Ummartyotin, S.; Tangnorawich, B. Utilization of eggshell waste as raw material for synthesis of hydroxyapatite. *Colloid Polym. Sci.* **2015**, *293*, 2477–2483. [CrossRef]
48. Marr, I.L. Separation and spectrophotometric determination of elements. *Endeavour* **1987**, *11*, 220. [CrossRef]
49. Goddard, A.F.; Jessa, M.J.; Barrett, D.A.; Shaw, P.N.; Idstrom, J.P.; Cederberg, C.; Spiller, R.C. Effect of omeprazole on the distribution of metronidazole, amoxicillin, and clarithromycin in human gastric juice. *Gastroenterology* **1996**, *111*, 358–367. [CrossRef]
50. Adriano, W.S.; Veredas, V.; Santana, C.C.; Gonçalves, L.R.B. Adsorption of amoxicillin on chitosan beads: Kinetics, equilibrium and validation of finite bath models. *Biochem. Eng. J.* **2005**, *27*, 132–137. [CrossRef]
51. Ahmed, M.B.; Zhou, J.L.; Ngo, H.H.; Guo, W. Adsorptive removal of antibiotics from water and wastewater: Progress and challenges. *Sci. Total Environ.* **2015**, *532*, 112–126. [CrossRef] [PubMed]
52. Dastgheib, S.A.; Rockstraw, D.A. A systematic study and proposed model of the adsorption of binary metal ion solutes in aqueous solution onto activated carbon produced from Pecan Shells. *Carbon* **2002**, *40*, 1853–1861. [CrossRef]
53. Al-Saidi, H.M.; Abdel-Fadeel, M.A.; El-Sonbati, A.Z.; El-Bindary, A.A. Multi-walled carbon nanotubes as an adsorbent material for the solid phase extraction of bismuth from aqueous media: Kinetic and thermodynamic studies and analytical applications. *J. Mol. Liq.* **2016**, *216*, 693–698. [CrossRef]
54. Weber, W.J.; Morris, J.C. Kinetics of adsorption on carbon from solution. *J. Sanit. Eng. Div.* **1963**, *89*, 31–59. [CrossRef]
55. Dalal, R.C. Desorption of soil phosphate by anion-exchange resin. *Commun. Soil Sci. Plant Anal.* **1974**, *5*, 531–538. [CrossRef]
56. Bhattacharya, A.K.; Venkobachar, C. Removal of cadmium (ii) by low cost adsorbents. *J. Environ. Eng.* **1984**, *110*, 110–122. [CrossRef]
57. Salam, M.A.; Alkhateeb, L.; Abdel-Fadeel, M.A. Removal of toxic ammonium ions from water using nanographene sheets. *Desalination Water Treat.* **2018**, *129*, 168–176. [CrossRef]
58. Dubinin, M.M. The surface and porosity of adsorbents. *Bull. Acad. Sci. USSR Div. Chem. Sci.* **1974**, *23*, 958–971. [CrossRef]
59. Reichenberg, D. Properties of ion-exchange resins in relation to their structure. III. Kinetics of Exchange. *J. Am. Chem. Soc.* **1953**, *75*, 589–597. [CrossRef]
60. Hameed, S.A.; Abdel-Fadeel, M.A.; Al-Saidi, H.M.; Abdel Salam, M. Simultaneous removal of the toxic tungsten ions and rhodamine B dye by graphene nanosheets from model and real water. *Desalination Water Treat.* **2020**, *188*, 266–276. [CrossRef]
61. Chaba, J.M.; Nomngongo, P.N. Effective adsorptive removal of amoxicillin from aqueous solutions and wastewater samples using zinc oxide coated carbon nanofiber composite. *Emerg. Contam.* **2019**, *5*, 143–149. [CrossRef]
62. Kakavandi, B.; Esrafili, A.; Mohseni-Bandpi, A.; Jonidi Jafari, A.; Rezaei Kalantary, R. Magnetic $Fe_3O_4$@C nanoparticles as adsorbents for removal of amoxicillin from aqueous solution. *Water Sci. Technol.* **2013**, *69*, 147–155. [CrossRef] [PubMed]
63. Moradi, O.; Alizadeh, H.; Sedaghat, S. Removal of pharmaceuticals (diclofenac and amoxicillin) by maltodextrin/reduced graphene and maltodextrin/reduced graphene/copper oxide nanocomposites. *Chemosphere* **2022**, *299*, 134435. [CrossRef] [PubMed]
64. Lotfollahzadeh, R.; Yari, M.; Sedaghat, S.; Delbari, A.S. Biosynthesis and characterization of silver nanoparticles for the removal of amoxicillin from aqueous solutions using Oenothera biennis water extract. *J. Nanostructure Chem.* **2021**, *11*, 693–706. [CrossRef]
65. Mahmodi Sheikh Sarmast, Z.; Sedaghat, S.; Derakhshi, P.; Azar, P.A. Facile fabrication of silver nanoparticles grafted with fe3o4-chitosan for efficient removal of amoxicillin from aqueous solution: Application of central composite design. *J. Polym. Environ.* **2022**, *30*, 2990–3004. [CrossRef]
66. Caravaca, M.; Vicente-Martínez, Y.; Soto-Meca, A.; Angulo-González, E. Total removal of amoxicillin from water using magnetic core nanoparticles functionalized with silver. *Environ. Res.* **2022**, *211*, 113091. [CrossRef]
67. Jalees, M.I.; Nawaz, R. Synthesis and application of $MOS_2$ nanosheets for the removal of amoxicillin from water: Response surface method. *Arab. J. Sci. Eng.* **2022**, *48*, 443–455. [CrossRef]
68. Bisaria, K.; Wadhwa, S.; Mathur, A.; Roy, S.; Dixit, A.; Singh, R. New bismuth oxyiodide/chitosan nanocomposite for ultrasonic waves expedited adsorptive removal of amoxicillin from aqueous medium: Kinetic, isotherm and thermodynamic investigations. *Environ. Sci. Pollut. Res.* **2022**, *29*, 86260–86276. [CrossRef]